Many-body pseudopotential theory of excitons in InP and CdSe quantum dots

A. Franceschetti, H. Fu, L. W. Wang, and A. Zunger
National Renewable Energy Laboratory, Golden, Colorado 80401
~Received 15 October 1998!

We present a pseudopotential approach to the calculation of the excitonic spectrum of semiconductor quantum dots. Starting from a many-body expansion of the exciton wave functions in terms of single-substitution Slater determinants constructed from pseudopotential single-particle wave functions, our method permits an accurate and detailed treatment of the intraconfiguration electron-hole Coulomb and exchange interactions, while correlation effects can be included in a controlled fashion by allowing interconfiguration coupling. We calculate the exciton fine structure of InP and CdSe nanocrystals in the strong-confinement regime. We find a different size dependence for the electron-hole exchange interaction than previously assumed ~i.e., R^{-2} instead of R^{-3}). Our calculated exciton fine structure is compared with recent experimental results obtained by size-selective optical spectroscopies. @S0163-1829~99!00227-1#

I. INTRODUCTION

The physics of excitons in *bulk semiconductors*[1] is governed by electron-hole *correlation* effects, which control the magnitude of the exciton radius and exciton binding energy. A departure from this 1 1 1

model Hamiltonian fit well the observed redshift in CdSe nanocrystals,[6,8,9]

$$J_{vc,v'c'}=e^2\sum_{s_1,s_2}\int\int\frac{\psi^*_{v'}(\mathbf{r}_1,s_1)\psi^*_c(\mathbf{r}_2,s_2)\psi_v(\mathbf{r}_1,s_1)\psi_{c'}(\mathbf{r}_2,s_2)}{\bar{\epsilon}(\mathbf{r}_1,\mathbf{r}_2)|\mathbf{r}_1-\mathbf{r}_2|}d\mathbf{r}_1d\mathbf{r}_2, \quad (6)$$

$$K_{vc,v'c'}=e^2\sum_{s_1,s_2}\int\int\frac{\psi^*_{v'}(\mathbf{r}_1,s_1)\psi^*_c(\mathbf{r}_2,s_2)\psi_{c'}(\mathbf{r}_1,s_1)\psi_v(\mathbf{r}_2,s_2)}{\bar{\epsilon}(\mathbf{r}_1,\mathbf{r}_2)|\mathbf{r}_1-\mathbf{r}_2|}d\mathbf{r}_1d\mathbf{r}_2. \quad (7)$$

The screening of the electron-hole interaction, caused by the polarization of the medium, is described phenomenologically by the *microscopic*, position-dependent dielectric constant $\bar{\epsilon}$ and will be discussed in Sec. II B. The structure of the Hamiltonian matrix is schematically illustrated in Fig. 1. The diagonal blocks (shaded areas) correspond to matrix elements $\mathcal{H}_{vc,v'c'}$ between Slater determinants belonging to the same configuration. The off-diagonal blocks (unshaded areas) describe the coupling between different configurations.

The excitonic states of the quantum dot are obtained by solving the secular equation

$$\sum_{v'=1}^{N_v}\sum_{c'=1}^{N_c}\mathcal{H}_{vc,v'c'}C^{(\alpha)}_{v',c'}=E^{(\alpha)}C^{(\alpha)}_{v,c}. \quad (8)$$

From the knowledge of the exciton energy levels and wave functions, the near-edge normalized absorption spectrum can be obtained as

$$\sigma(\omega)\propto\frac{1}{V}\sum_{\alpha}|\mathbf{M}^{(\alpha)}|^2\delta(\hbar\omega-E^{(\alpha)}), \quad (9)$$

where V is the nanocrystal volume and $\mathbf{M}^{(\alpha)}$ are the dipole matrix elements:

$$\mathbf{M}^{(\alpha)}=\sum_{vc}C^{(\alpha)}_{v,c}\langle\psi_v|\mathbf{r}|\psi_c\rangle. \quad (10)$$

In the following sections the most important details of the solution of Eqs. (1)–(10) will be discussed.

A. Solution of the single-particle problem

The solution of the Schrödinger equation (1) for a 1000-atom system represents a formidable task, even when a fixed, non-self-consistent potential is used. However, only a few single-particle states in an energy window around the band gap are needed in the construction of the basis set $\{\Phi_{v,c}\}$. Thus, Eq. (1) can be effectively solved using the folded spectrum method,[26,27] which allows one to calculate *selected* eigenstates of the Schrödinger equation. In this approach, Eq. (1) is replaced by the eigenvalue equation

$$\left[-\frac{\hbar^2}{2m}\nabla^2+V_{\rm ps}(\mathbf{r})+\hat{V}_{\rm NL}-\epsilon_{\rm ref}\right]^2\psi_i(\mathbf{r},s)$$
$$=(\epsilon_i-\epsilon_{\rm ref})^2\psi_i(\mathbf{r},s), \quad (11)$$

where $\epsilon_{\rm ref}$ is an *arbitrary* reference energy. The "ground state" of Eq. (11) coincides with the solution of the Schrödinger equation (1) with energy closest to the reference energy $\epsilon_{\rm ref}$. Therefore, by choosing the reference energy in the band gap, the band-edge states can be obtained by minimizing the functional $A[\psi]=\langle\psi|(\hat{H}-\epsilon_{\rm ref})^2|\psi\rangle$.

We solve Eq. (11) by expanding the pseudopotential wave functions $\psi_i(\mathbf{r},s)$ in a plane-wave basis set. To this purpose, the total pseudopotential $V_{\rm ps}(\mathbf{r})$ is defined in a periodically repeated supercell Ω containing the quantum dot surrounded by a region of vacuum. The size of the vacuum region is sufficiently large to ensure that the solutions of Eq. (11) are converged within a few meV. The single-particle wave functions can then be expanded as $\psi_i(\mathbf{r},s)=\sum_{\mathbf{G}}c_i(\mathbf{G},s)$985462.54 /F9 1 Te
. climi

structure and their overall symmetry is T_d. The CdSe nanocrystals have the wurtzite crystalline structure. In both cases, the interatomic distance is taken as the experimental bulk interatomic distance. The dangling bonds at the surface of

functions ~see Table I!. The ($h5$,$e1$) electron-hole pair of InP nanocrystals is optically active, as shown in Fig. 2, because the $h5$ single-particle state originates mainly from the

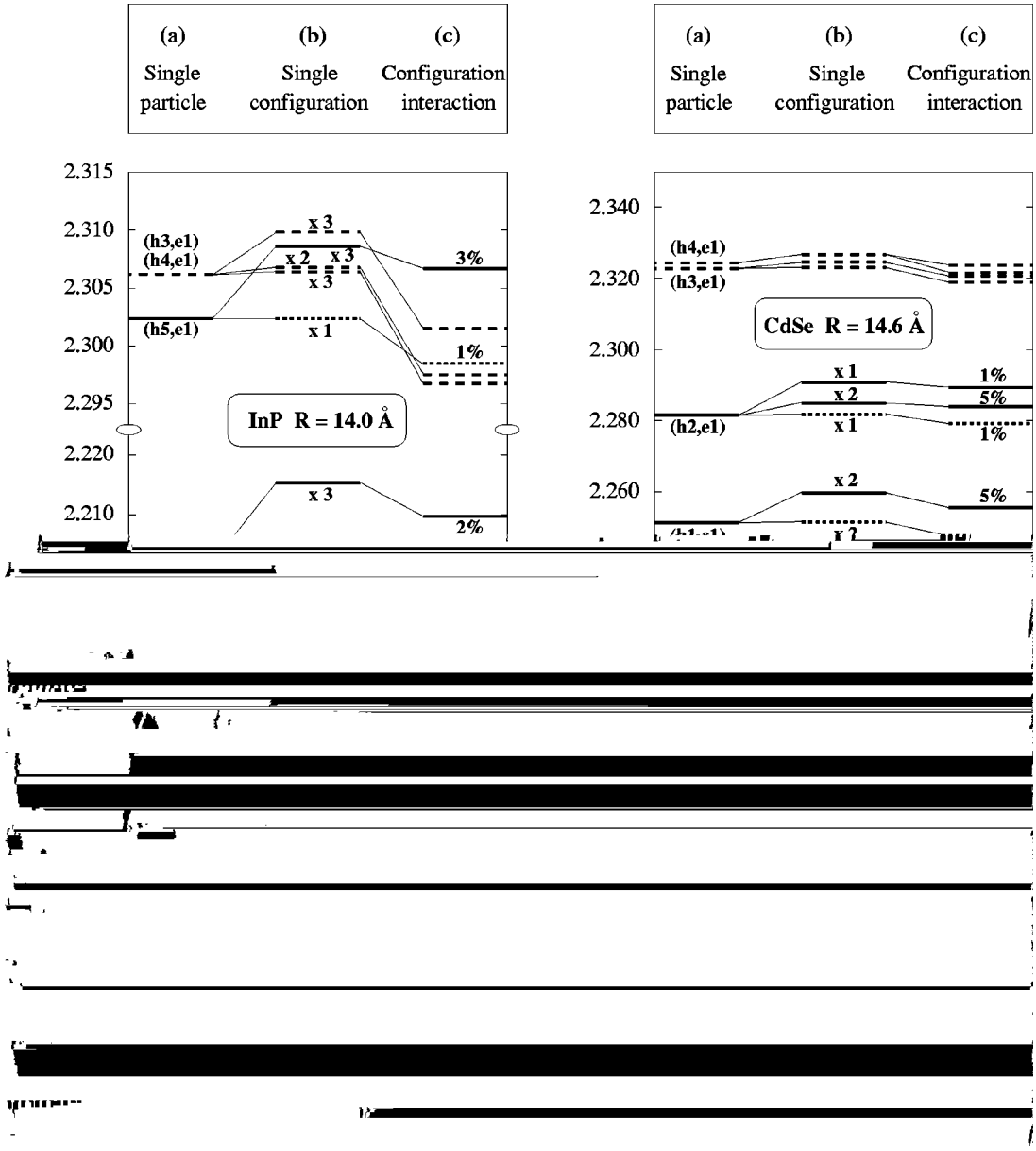

FIG. 3. ~a! Single-particle spectrum of InP and CdSe nanocrystals including Coulomb interaction. ~b! Single-configuration spectrum. ~c! Configuration-interaction spectrum. Solid lines denote optically active states, dashed lines denote orbitally-forbidden states, dotted lines denote spin-forbidden states. The symbols in parentheses in ~a! denote the electron-hole pairs from which the exciton states originate. The degeneracy of each exciton level in the single-configuration approximation is shown in ~b!. The configuration-mixing coefficients $c_i^{(a)}$ ~see Eq. ~18!# are shown in ~c!. The total number of single-particle states included in the configuration-interaction expansion is 26 valence states and 18 conduction states for the $R=14.0$ Å InP nanocrystal, 22 valence states and 10 conduction states for the $R=17.4$ Å InP nanocrystal, 8 valence states and 8 conduction states for the two CdSe nanocrystals.

in the single-particle approximation, the order is reversed when the Coulomb interaction is included ~see Fig. 2!.

C. Single-configuration approximation

In the ''single-configuration'' approach, only the diagonal blocks of the Hamiltonian matrix $\mathcal{H}_{vc,v'c'}$ ~shaded areas in Fig. 1! are retained. The intraconfiguration Coulomb and exchange matrix elements are fully included in the single-configuration calculation, whereas the interaction between different configurations ~nonshaded areas in Fig. 1! is neglected. This approach was used by Efros *et al.*[9] in the context of the $\mathbf{k}\cdot\mathbf{p}$ approximation to analyze the splitting of the lowest-energy exciton in CdSe nanocrystals.

The single-configuration spectrum of InP and CdSe nanocrystals is shown in Fig. 3~b!. While the effects of the intraconfiguration Coulomb interaction are negligible, the exciton levels are split by the intraconfiguration exchange interaction into a lower-energy, spin-forbidden multiplet ~dotted lines!, and a higher-energy, spin-allowed multiplet ~solid lines!. This splitting creates the exciton ''fine structure.''

D. Configuration-interaction spectrum

In the final step, the configuration-interaction spectrum is obtained by diagonalizing the Hamiltonian matrix of Eq. ~5!. The convergence of the configuration-interaction expansion

in terms of the size of the determinantal basis set is illustrated in Fig. 4. This figure shows a contour plot of the lowest exciton energy of an InP nanocrystal ($R=14.0$ Å) as a function of the number of valence states (N_v) and conduction states (N_c) included in the many-body expansion of Eq. ~4!. As we can see from Fig. 4, the convergence of the exciton energy levels is quite slow. The convergence of the level splittings, however, is relatively fast. We estimate that the calculated exchange splitting of the lowest-energy exciton state is converged within 0.5 meV for the nanocrystals considered here. The splitting of higher-energy exciton states is converged within a few meV.

The extent of configuration mixing can be quantified by defining the mixing coefficient

$$\eta^{(a)} = 1 - \sum_{v,c} |C_{v,c}^{(a)}|^2, \qquad \text{~18!}$$

where the sum is restricted to the Slater determinants belonging to the single configuration from which the exciton state $C^{(a)}$ predominantly originates. The energy spectrum including configuration-interaction effects is shown in Fig. 3~c!. The main consequence of configuration mixing is a significant downshift ~several meV! of the energy levels. In some cases level crossing can be observed, although the configuration mixing is relatively small ($\eta^{(a)} < 5\%$ in all the cases considered here!. Interestingly, we find that the lowest excitonic state is essentially spin forbidden, even when configuration mixing is included. In fact, the ratio between the transition probabilities of the lowest allowed transition and the lowest forbidden transition is at least 10^6 in CdSe nanocrystals and 10^{10} in InP nanocrystals. This is in contrast with the results of Leung *et al.*[20] who found a ratio of about 10^3 in the case of CdSe spherical nanocrystals. The allowed/forbidden ratio may depend strongly on the shape of the nanocrystal.

IV. ANALYSIS OF THE BAND-EDGE EXCITON LEVELS

A. Exciton energies

In a semiconductor nanocrystal with T_d symmetry the Γ_{8v} valence-band maximum is four-fold degenerate, while the Γ_{6c} conduction-band minimum is twofold degenerate ~including spin degeneracy!. Thus, in the absence of electron-hole interaction, the lowest exciton level is eightfold degenerate. This degeneracy can be broken by deviations from the T_d symmetry and/or by the electron-hole interaction.

Using a perturbative approach ~which neglects configuration interactions!, Efros *et al.*[9] have shown that the lowest exciton eightfold multiplet splits into five different energy levels, which are labeled ~subscripts! according to their total angular momentum projection F:

$$E_{\pm 2} = -\frac{3}{2}\Delta_X - \frac{1}{2}\Delta_{\mathrm{CF}},$$

$$E_{\pm 1}^{L} = \frac{1}{2}\Delta_X - \sqrt{\frac{(2\Delta_X - \Delta_{\mathrm{CF}})^2}{4} + 3\Delta_X^2},$$

$$E_{\pm 1}^{U} = \frac{1}{2}\Delta_X + \sqrt{\frac{(2\Delta_X - \Delta_{\mathrm{CF}})^2}{4} + 3\Delta_X^2}, \qquad \text{~19!}$$

$$E_{0}^{L} = -\frac{3}{2}\Delta_X + \frac{1}{2}\Delta_{\mathrm{CF}},$$

$$E_{0}^{U} = \frac{5}{2}\Delta_X + \frac{1}{2}\Delta_{\mathrm{CF}},$$

where Δ_X

meV. Our results are summarized in Table II. We next compare our results with previous calculations and with experiment.

B. Comparison with previous calculations

In the phenomenological approach used by Norris *et al.*,[6] Nirmal *et al.*,[8] Efros *et al.*,[9] Chamarro *et al.*,[10] and Woggon *et al.*,[11] the exchange parameter D_X was calculated retaining only the short-range part of the electron-hole exchange interaction and, therefore, assuming that the exchange parameter scales as $1/R^3$ with the nanocrystal size. Also, the crystal-field contribution to D_{CF} was assumed to be size independent.

The last column of Table II shows the exchange parameter D_X^{EMA} for CdSe nanocrystals, calculated according to the effective-mass model of Efros *et al.*[9] We see that D_X^{EMA} is significantly overestimated compared to the direct pseudopotential calculation. By fitting the *size dependence* of our calculated exchange energy with the functional form $D_X(R) = aR^{-g}$, we obtain $g = 1.93$ for InP nanocrystals[36] and $g = 1.97$ for CdSe nanocrystals. This is in contrast with the conventional assumption[6,8–10] that D_X scales as R^{-3}. The reason for this discrepancy is the presence of a sizable long-range component in the electron-hole exchange interaction.[23] Banin *et al.*[12] found experimentally that the exchange splitting in InAs nanocrystals scales approximately as R^{-2}. They interpreted their results in the framework of the effective-mass approximation by assuming the existence of a significant leakage of the electron wave function outside the nanocrystal. The resulting exchange parameter was then multiplied by an adjustable prefactor and fitted to the experimental exchange splitting. This model, however, ignores the long-range contributions to D_X, which are responsible for the R^{-2} scaling.

C. Comparison with experiment

The exciton splitting of InP nanocrystals calculated using pseudopotential wave functions is compared in Fig. 5 with a fit to the experimental results of Micic *et al.*[7] As we can see, the agreement with experimental results is very good and

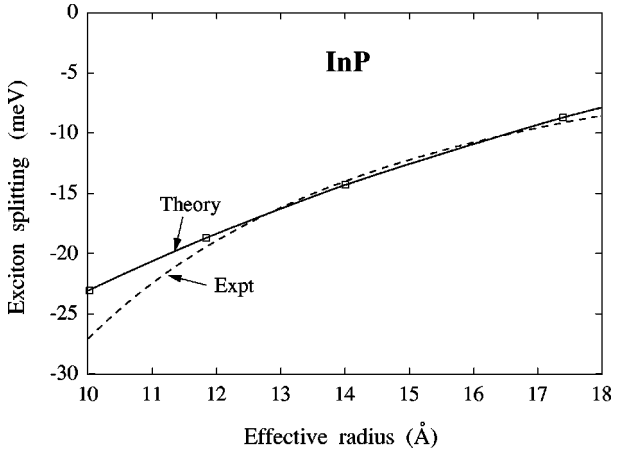

FIG. 5. The pseudopotential calculated exciton splitting of spherical InP nanocrystals ~solid line! is compared with a fit to the experimental results of Micic *et al.* ~Ref. 7, dashed line!. The energy of the lowest spin-allowed optical transition is taken as the zero of the energy scale.

indicates that the observed redshift of the emission peak originates from the exciton exchange splitting.

Figure 6 compares the calculated low-energy excitonic levels of CdSe nanocrystals with the experimental results of Norris *et al.*[6] The exciton energies are plotted as a function of the band-gap energy ~corresponding to the energy of the lowest absorbing state!, as the measured nanocrystal size is subject to significant uncertainty. The two exciton levels $E_{\pm 1}^U$ and E_0^U are not resolved experimentally for small nanocrystals ~band gap >2.1 eV), so their average is shown in Fig. 6. The agreement between theory and experiment is very good, although some discrepancies seem to exist for large nanocrystals ~band gap <2 eV!. We observe, however, that in the bulk limit the exciton levels $E_{\pm 2}$ and $E_{\pm 1}^L$ should converge to $E=0$, while the levels E_0^L, $E_{\pm 1}^U$, and E_0^U should

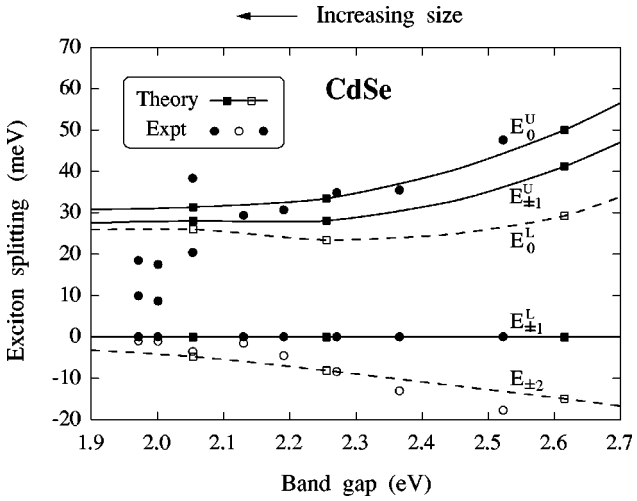

FIG. 6. Comparison of calculated ~squares joined by lines! and measured ~circles! excitonic levels of Cd-316.379.1(en-)Tj 26.379.1(en-256cant)-

converge to the value of the bulk crystal-field splitting, $E = 26$ meV. The experimental exciton energies for large nanocrystals do not appear to approach the bulk limit in a consistent way.

V. SUMMARY

Using a many-body expansion based on *microscopic* pseudopotential wave functions, we have developed a practical and accurate method to calculate the excitonic spectrum of semiconductor quantum dots in the strong-confinement regime. We find that ~i! the diagonal Coulomb energies $J_{v,c}$ depend on the electron and hole orbitals. This effect leads in some cases to level crossing ~Fig. 2!. ~ii! Intraconfiguration exchange leads to splitting into spin-forbidden and spin-allowed multiplets ~Fig. 3!. ~iii! Configuration mixing leads to significant energy lowering and possibly to state crossing ~Fig. 3!. If configuration interactions are ignored, the excitonic energy levels are off by several meV. ~iv! Configuration mixing does not significantly affect the oscillator strength of the lowest, spin-forbidden excitonic multiplet. ~v! The phenomenological single-configuration model of Efros *et al.*[9] is analyzed. We find that the exchange parameter $D_X(R)$ has a different size dependence than previously assumed.[9]

ACKNOWLEDGMENTS

This work was supported by the U.S. DOE, OER-BES, Division of Materials Science, under Grant No. DE-AC36-98-GO 10337.

APPENDIX

In this appendix we discuss a practical and accurate method to accelerate the convergence of the reciprocal-space expansion of Coulomb @Eq. ~6!# and exchange @Eq. ~7!# integrals with respect to the volume V of the supercell containing the quantum dot and the surrounding barrier. In the reciprocal-space formalism @see Eqs. ~16! and ~17!#, these integrals have the general form

$$E(V) = \int_V \rho_1^*(\mathbf{G})\, g(\mathbf{G})\, \rho_2(\mathbf{G}), \qquad \text{(A1)}$$

where $\rho_1(\mathbf{G})$, $\rho_2(\mathbf{G})$, and $g(\mathbf{G})$ are the Fourier transforms of $\rho_1(\mathbf{r})$, $\rho_2(\mathbf{r})$, and $g(\mathbf{r}-\mathbf{r}')$, respectively, and the sum runs over the reciprocal-lattice vectors $\mathbf{G}$ of the supercell V.

The convergence of the Fourier expansion

ing to $V \to \infty$). The expansion of Eq. (A3) works well whenever the electrostatic interaction between the periodic replicas of the quantum dots—described by the long-range part of the function $g(\mathbf{r}-\mathbf{r}')$—is essentially Coulombic. This includes the cases where the screening function $\bar{\epsilon}(\mathbf{r}-\mathbf{r}')$ of Eq. (12) is a constant or converges rapidly (within a few lattice constants) to its asymptotic ($|\mathbf{r}-\mathbf{r}'| \to \infty$) limit.

In the presence of strong ionic screening, however, the long-range part of $g(\mathbf{r}-\mathbf{r}')$ can deviate considerably from a simple $1/r$ function. In this case the corrected integrals (A3) converge slowly with the supercell size, particularly when $q_1 = q_2 = 1$. It is then more convenient to use a truncated form of the screened Coulomb interaction

$$g$$